Wood Science and Technology 33 (1999) 445–464

The use of numerical simulation as a cognitive tool for studying the microwave drying of softwood in an over-sized waveguide

P. Perré, I. W. Turner

Abstract A previously developed mathematical model, which uses a comprehensive two-dimensional heat and mass transport code coupled with a three-dimensional code for resolving Maxwell's equations in the time domain, will be used to investigate numerous aspects of the microwave enhanced convective drying of softwood in an over-sized waveguide. At first, in order to highlight the predictive capabilities of the developed model, comparisons will be made between theory and experiment for spruce heartwood. It will be shown that the model is able to identify most of the important heat and mass transfer phenomena that arise throughout the drying process. After validation of the numerical simulation results, the work focuses on using the model as a cognitive tool for investigating important issues for closed microwave systems which include the effect of varying the sample dimensions and changing the location of the material within the applicator. Finally, a study will be presented that compares the overall drying kinetics generated within two different types of applicator designs. The first design uses a wave-trap located at the end of the waveguide to prevent reflected energy from back-propagating into the over-sized section of the guide, while the second design uses a short-circuit plane to ensure that this

Received 25 May 1997

P. Perré
E.N.G.R.E.F. – Laboratory of Forest Sciences,
Forest Products Team, 14 rue Girardet,
F-54042 Nancy Cedex, France

I. W. Turner
School of Mathematics, Queensland University of Technology,
GPO Box 2434, Brisbane, Q4001, Australia

One of the authors, Ian Turner, would like to thank CSR Softwoods, Queensland Pty Ltd of Australia for their continuing support of this work. He would also like to thank the ENGREF for supporting his sabbatical stay in Nancy, France. Both authors would also like to thank Prof. Roques for allowing the use of the over-sized waveguide to perform the experiments. The computations referred to in this paper were carried out on computing equipment supplied to the School of Mathematics, Queensland University of Technology, under the Digital Equipment Agreement ERP No. 2057. This work was also supported by an ARC Collaborative Research Grant scheme from the Australian Government

reflected energy is back – propagated towards the material. The advantages and disadvantages of these two designs will be deliberated.

List of symbols

c	Speed of light in vacuum, m s^{-3}
B	Magnetic flux intensity, T
E	Electric field vector, V m^{-3}
H	Magnetic field vector, A m^{-3}
J	Flux vector, kg m^{-2} s^{-1}
$\overline{\overline{\mathbf{K}}}$	Kinetic transport tensor
P_{inc}	Incident power, W m^{-2}
S	Saturation
T	Temperature, K
t	time, s

Greek symbols

ε_o	Permittivity of free space, F m^{-3}
ε'	Relative dielectric constant
ε''	Relative loss factor
Φ	Porosity, m^3 m^{-3}
φ	Phase potential
Φ	Volumetric source term, W m^{-3}
Ψ	Conserved quantity
μ_b	Chemical potential, J kg^{-1}
ρ	Intrinsic averaged density, kg m^{-3}
σ	Effective conductivity, S m^{-1}
ω	Mass fraction
ν	Frequency, Hz

Subscripts

a	Air
e	Effective property
g	Gas phase
l	Liquid phase
v	Vapour
0	Atmospheric value

Introduction

It is now well known that dielectrically assisted drying processes can provide numerous advantages over classical convective drying techniques. Some of these advantages include: volumetric heating, moisture levelling, increased liquid and vapour migration from the interior to the surface of the product and in some cases, superior end-product quality. Although combined microwave and convective drying of wood is an innovative drying strategy that can offer these benefits over standard kiln drying methods, little research impetus has been focused on the modelling of this process at a fundamental level. The complicated physics that arise throughout the drying process, together with the lack of knowledge of how the wood and the microwave fields interact during the heating

process, have caused researchers to avoid the challenge of developing a complete model to describe combined microwave and convective drying. In this work, a previously developed completely coupled drying model (Perré and Turner, 1996; Perré and Turner, 1997), that combines Maxwell's electromagnetic equations with an existing comprehensive two-dimensional heat and mass transfer model, is used to investigate some important aspects of microwave enhanced convective drying of softwood in an over-sized waveguide. The solution of the Maxwell equations is performed in the time domain by using the Finite Difference Time Domain (FD-TD) technique (De Pourcq, 1985; Lui et al., 1994; Turner, 1994; Liu and Turner, 1995; Lui et al., 1996; Zhao and Turner, 1996) and the resolution of the heat and mass transport model (TRANSPORE) is based entirely on the numerical strategies that have been documented in prior research work by the authors (Perré and Degiovanni, 1990; Perré et al., 1993, Turner and Perré, 1995; Turner and Perré; Perré and Turner, 1996). The combination of the TRANSPORE and FD-TD models allows, for possibly the first time, the complete mathematical description of the microwave heating phenomena which evolve inside the waveguide throughout the dielectric drying process.

The over-sized waveguide system exhibited in Fig. 1 operates by propagating travelling waves along the z-direction of the waveguide towards a water load that is situated at the end of the guide. The water load ensures that only a minimal amount of energy is reflected back to the sample, while an iso-circulator located at the front end of the guide is used to trap any energy reflected from the sample damaging the magnetron. The wood sample is inserted in the central over-sized section of the guide. As the microwave heating proceeds, the wood absorbs a certain amount of energy from the exponentially decaying travelling microwave field in accordance with the properties of its effective loss factor.

Because the water that is distributed throughout the complex wood pore structure couples very well with the electromagnetic fields that evolve inside the waveguide, the energy from the microwaves can be transmitted directly to the bulk of the wet sample. In this case, the medium no longer relies on the external

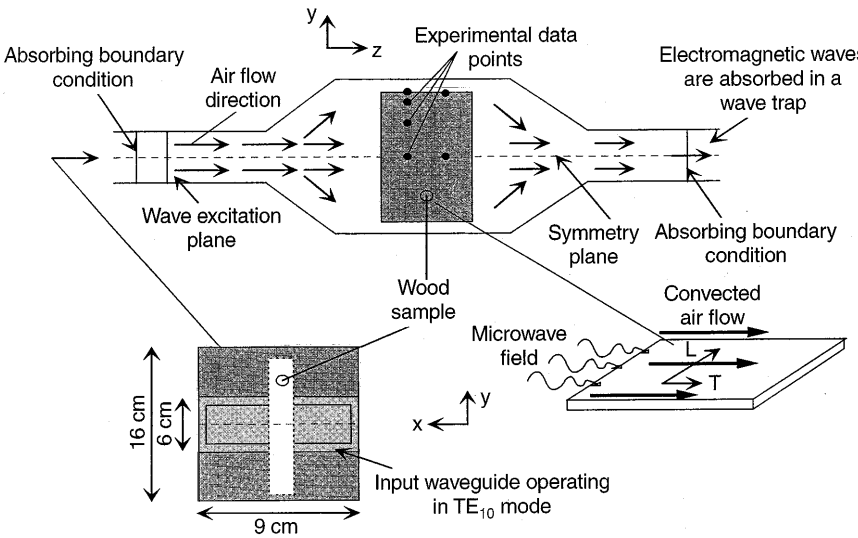

Fig. 1. Schematic of the over-sized waveguide used for this analysis

convective air characteristics for drying. Instead, a volumetric heating effect manifests itself within the wood. Furthermore, due to this rapid heating process, a large internal vapour pressure can increase substantially the liquid extraction rate from the wood by means of what is known as a pumping phenomenon. Finally, due to the fact that during microwave heating the surface of the wood is often cooled by evaporation, the resulting thermal gradients also can assist with mass diffusion. All of these facts inevitably result in a highly effective and efficient drying process.

The following chapters of this paper include a brief description of the mathematical model that was proposed previously (Perré and Turner, 1997), followed by a presentation of the results obtained from the simulations carried out using that model. In order to demonstrate the capabilities of the developed software, a comparison is made with an experimental data set pertaining to the microwave – enhanced convective drying of spruce heartwood. The experiments were conducted in a small scale over-sized waveguide whose detailed description can be found elsewhere (Constant, 1992; Constant et al., 1996). Following from these discussions, a study is given which analyses the impact that varying product size or location within the waveguide can have on the efficiency of the drying process. Finally, the effect of using a short circuit plane rather than a water load at the end of the waveguide will be investigated in an attempt to determine if one design offers any operational advantages over the other.

Mathematical formulation

The equations used to mathematically model the physics of drying originate from the pioneering work of Whitaker (1977) and can be cast succinctly into a generalised form that involves all of the necessary migration mechanisms to allow an adequate description of the evolution of the free liquid, bound liquid and gas phases which coexist within the infrastructure of the porous medium (Turner and Perré, 1996):

$$\frac{\partial \Psi}{\partial t} - \nabla \cdot \mathbf{J} = \Phi \text{ where}$$

$$\mathbf{J} = \overline{\overline{\mathbf{K}}}_1 \nabla \varphi_w + \overline{\overline{\mathbf{K}}}_2 \nabla \varphi_g + \overline{\overline{\mathbf{K}}}_3 \nabla \omega_v + \overline{\overline{\mathbf{K}}}_4 \nabla \omega_a + \overline{\overline{\mathbf{K}}}_5 \nabla \mu_b + \overline{\overline{\mathbf{K}}}_6 \nabla T \qquad (1)$$

In Eq. (1) the term Ψ represents the conserved quantities of total liquid, energy or air, where for example, $\Psi_w = \phi S_w \rho_w + \phi S_g \rho_v + \overline{\rho}_b$ and the kinetic sensor terms denoted by $\overline{\overline{\mathbf{K}}}_i$ are complicated functions of the state system variables. Note further that not all of the driving potentials given in Eq. (1) are actually present in each of the macroscopic balance equations, nor are they all present for each drying state. A complete summary of the equations that govern the drying process, together with a comprehensive list of parameters used for the simulations can be found in Appendix 1.

The volumetric power density term Φ, which exists only in the energy balance equation, is given by

$$\Phi = \tfrac{1}{2} \sigma_e |\mathbf{E}|^2 \qquad (2)$$

where $\mathbf{E}$ is the electric field and σ_e the effective conductivity. Hence, it is clear that before the heat and mass transfer equations can be resolved numerically, the magnitude of the electric field within the material for the microwave applicator configuration shown in Fig. 1 must be determined. Unfortunately, an analytic

expression for the power density source term can be derived only for specialised applicator designs and typically, some form of numerical strategy becomes necessary. The literature indicates that three primary computational electromagnetic strategies exist. These strategies utilise finite differences – the FD-TD method (De Pourcq, 1985; Zhao and Turner, 1996), finite elements – the FE-TD method (Dibben and Metaxas, 1994) or discretise in space and solve a system of coupled differential equations – the method of Lines (Zhao et al., 1996). All three methods have their various advantages and disadvantages, however, the FD-TD philosophy appears to be simple to understand and straightforward to implement.

Most of the numerical strategies that are documented in the literature use the Maxwell equations as the starting point for their development, since these equations adequately describe an electromagnetic wave propagating in both time and space:

$$\nabla \times \mathbf{E} = -\frac{\partial \mathbf{B}}{\partial t}$$
$$\nabla \times \mathbf{H} = \frac{\partial \mathbf{D}}{\partial t} + \sigma_e \mathbf{E}$$
$$\nabla \cdot \mathbf{D} = \rho; \quad \nabla \cdot \mathbf{B} = 0$$
$$\mathbf{D} = \varepsilon \mathbf{E}; \quad \mathbf{B} = \mu \mathbf{H} \tag{3}$$

In Eqs. (3) the permeability μ, conductivity $\sigma_e = \omega\varepsilon_0\varepsilon''$ and permittivity $\varepsilon = \varepsilon_0\varepsilon'$ are time-independent real quantities that may vary from point to point, ε_0 is the free-space permittivity. In this work, since non-magnetic materials are being investigated, the permeability is assumed constant at the free space value $\mu = \mu_0$. However, here, the relative dielectric constant $\varepsilon'(X, T)$ and the relative dielectric loss factor $\varepsilon''(X, T)$ are assumed to vary with both moisture content and temperature during the drying process. The correlations for ε' and ε'' that were used in this work are taken directly from the literature (Chen and Pei, 1987) and represented graphically in Fig. 2.

Because the dielectric loss factor increases significantly with increasing moisture content, wet zones within the wood sample can be heated readily and as a

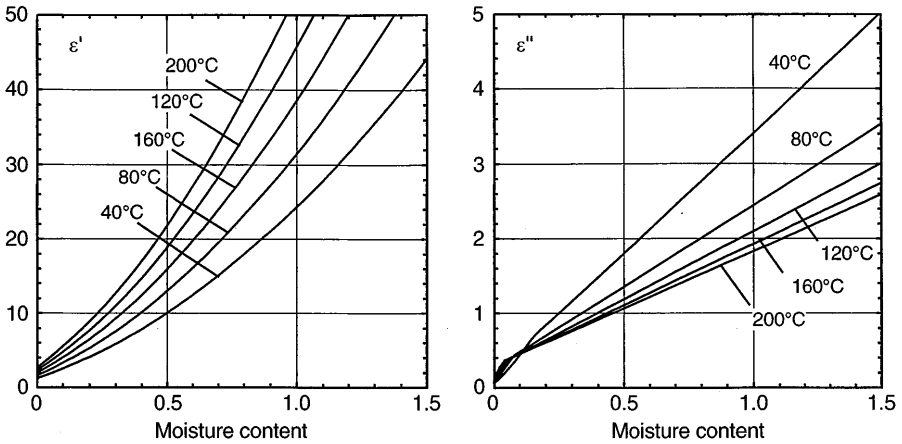

Fig. 2. Dielectric properties at different moisture contents (in%) used in the calculations

consequence, water evaporates more quickly than in dry zones. This moisture levelling phenomenon provides one of the most important benefits of the process from a quality view point. However, again due to the behaviour of the loss factor which often increases with temperature at low moisture contents, a thermal runaway effect can arise at locations where the standing wave configuration established within the material maximises the absorbed power. Indeed, this effect is one that is highly undesirable and one the model discussed here can predict.

A complete description of the numerical strategy used to couple the FD-TD model with the heat and mass transfer model TRANSPORE can be found in Perré and Turner (1997) and will not be repeated again here. Instead, the interested reader is referred to that previous work for further information.

Results and discussion

Experimental results

Figure 3 depicts the experimental results for the combined microwave and convective drying of spruce heartwood. The dimensions of the wood sample used for the experiment were 15 × 5.5 × 3.0 cm and the magnetron, which is connected to the waveguide, was configured to deliver incident powers up to 1000 W. However, for the experiments conducted for wood, only incident powers between 100–200 W were utilised. During the microwave experiments four distinct drying periods were identified. In period *1*, which is known as the heating period, the energy is transferred directly from the microwave field to the wood sample and very little mass loss is incurred. For period *2*, known as the streaming period, the temperature increases and passes through the boiling point of water and the resultant large internal vapour pressure drives the liquid from the medium quickly and efficiently under the action of pumping phenomenon.

During period *3*, which is known as the enthalpic period, the moisture content promptly decreases and under the influence of the elevated internal temperatures, vapour transport becomes the dominant migration mechanism because of the

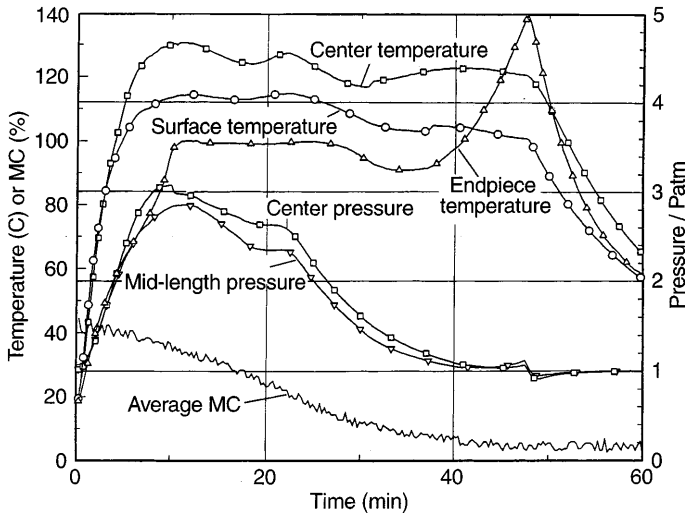

Fig. 3. Experimental results for combined microwave and convective drying of spruce heartwood (experimental incident power approximately 100 W)

sustained vaporisation that exists within the medium. The final period, known as the period of thermal runaway, commences when the medium becomes dry in certain locations and the temperature increases rapidly due to the characteristics of the dielectric loss factor that were explained in the preceding paragraphs. During this period, hot-spots and consequently, burning can become evident and the material can be severely damaged. For the present experiment, this phenomenon was apparent close to the end-piece of the sample, see Fig. 3. Interestingly, the thermal runaway effect was not observed in the centre or at the top surfaces of the board. At around 50 min of drying when the microwave power is turned off in order to avoid irrecoverable damage and burning of the sample, the temperatures begin to decrease and a small under-pressure due to vapour condensation becomes evident within the medium.

Numerical results

The surface area of the excitation port was such that the incident power for the experiment was approximately 2 kW m^{-2}. The amplitude of the incident electric field distribution was deduced using an ensuing classical correlation. The operation frequency was at the microwave level of 2.45 GHz. The input parameters used for the simulations are summarised in the Appendix A.2.

Figures 4 and 5 depict an example of the numerical results obtained using this very comprehensive numerical tool for a heartwood sample of spruce. The use of carpet plots allows the strong coupling of all variables to be highlighted: the absorbed power changes the temperature, which leads to an increase in both the vapor and total pressure gradients. These gradients induce, respectively, a diffusive vapor flux and convective gas and liquid fluxes that are responsible for the dramatic changes that arise within the moisture content distribution. In return, the overall changes in the dielectric properties impacts upon the standing wave patterns that exists within the sample. This phenomenon changes the power distribution which in turn affects the product temperature field and as a consequence, the cycle of the process continues. In fact, the strong coupling that exists between all physical variables within the model makes it necessary to recalculate the power each time the temperature or moisture content fields change significantly. From a physical point of view, it is to be noted that the coupling is so complicated that it becomes very difficult to deduce an accurate understanding of the process with coarse thinking. In particular, as opposed to what is sometimes documented in the drying literature, it is not necessarily the sections in the wood sample that have high moisture contents which absorb the majority of the energy supplied by the electromagnetic field. The leveling of the moisture content field is by far not easily predictable, and this is one of the main difficulties with the control of this heating process.

The proposed model was developed in order to take the intricate coupling phenomena into account, and it is apparent from Fig. 6 that the match between the experimental and theoretical results is qualitatively consistent, with the simulations exhibiting the same overall characteristic shape as the experimental profiles. In this figure, the thermal runaway seems to affect the whole length of material for z = 1.18 cm. In fact, the plotted nodes, which were chosen in order to be as close as possible to the experimental locations, do not provide a complete picture of what actually transpires within the sample throughout the drying process. Furthermore, closer observation of the generated carpet plots highlight that the model is able to capture the thermal runaway effect close to the end-piece of the board (Perré and Turner, 1996, 1997).

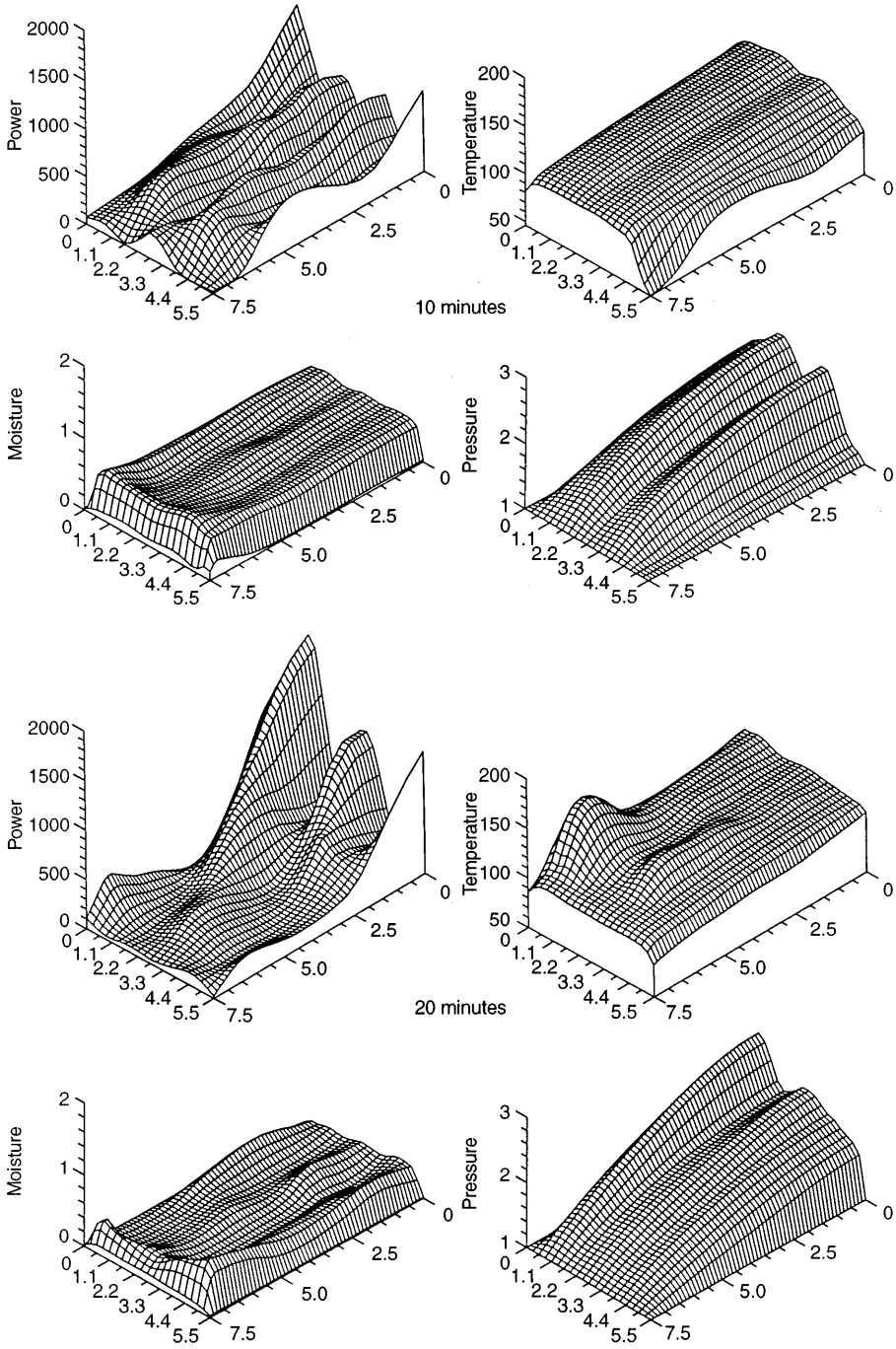

Fig. 4. Carpet plots of the power density, temperature, pressure and moisture content distributions at the times 10 and 20 minutes for heartwood

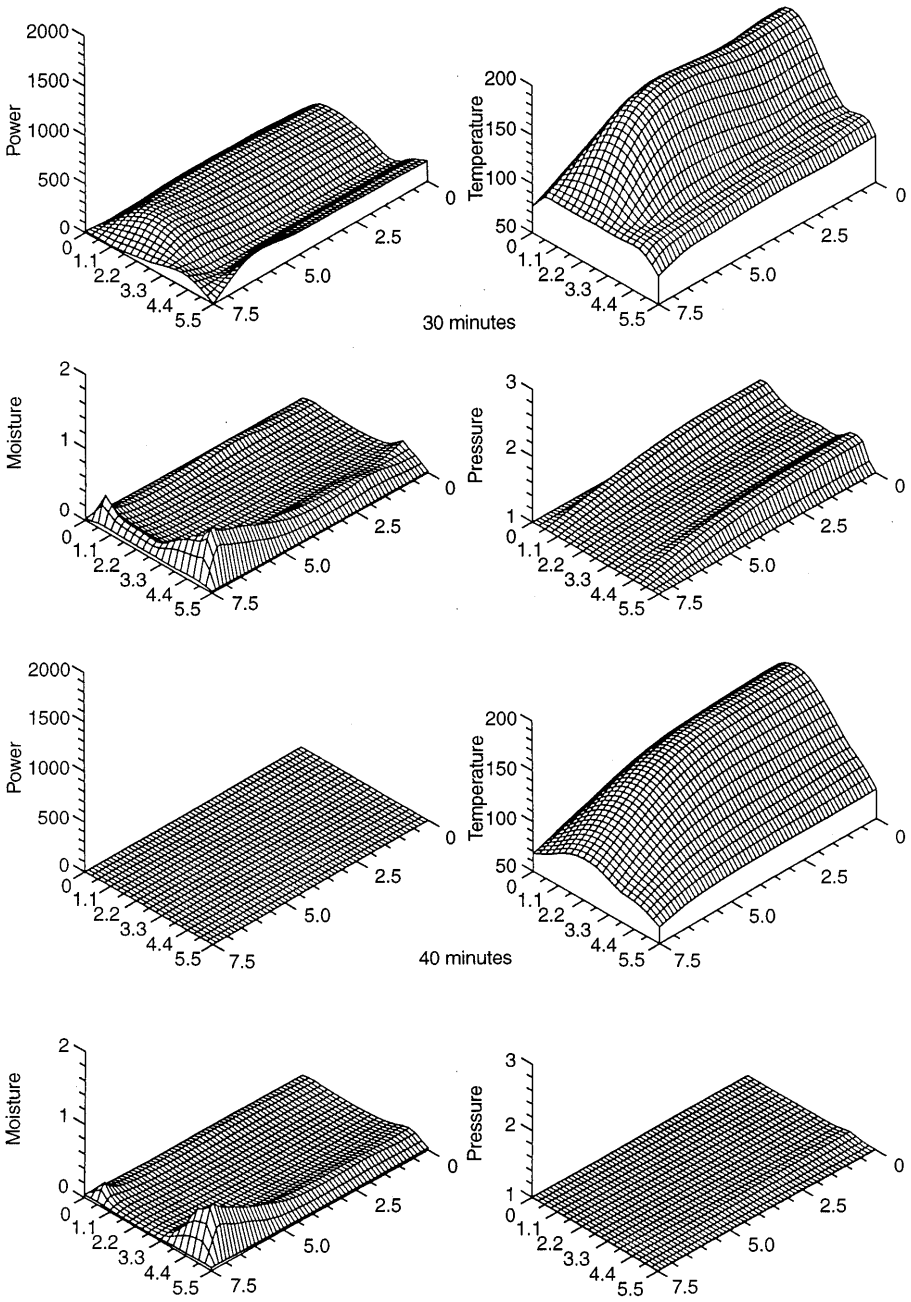

Fig. 5. Carpet plots of the power density, temperature, pressure and moisture content distributions at the times 30 and 40 minutes for heartwood

Although there are some differences between theory and experiment, it can be claimed that the coupled complete model represents reality more than adequately. Moreover, further observation of the kinetic curves depicted in Figs. 3 and 6 indicates that the overall drying times are approximately equivalent and that the

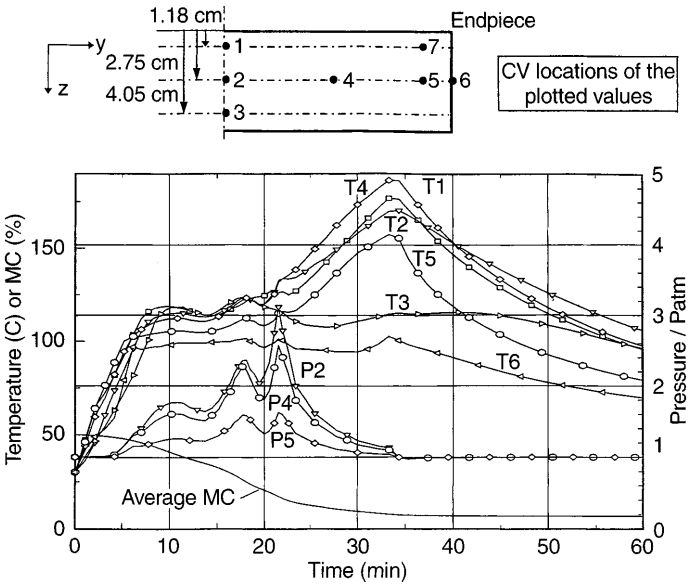

Fig. 6. Simulation results for combined microwave and convective drying of spruce heartwood

magnitude of the temperatures and pressures predicted within the sample are all close to the experimentally determined values. Another plausible explanation for any differences incurred between theory and experiment concerns the holes that were drilled in the sample for the positioning of the temperature and pressure sensors. Since the vapor is able to move freely along these holes, it is more likely that the sensor will measure the highest pressure and temperature registered throughout the hole, rather than strictly measure the value at the deepest location. Perhaps it would be more reasonable to take an averaging of the numerical results from the wood center (see for example point T2) through to the edge (see T1) when comparing the simulation and experimental results.

Figure 7 depicts a comparison between the experimentally measured power and the computed absorbed power for the wood throughout the drying process. Figure 7(a) indicates that during the first 20 min of drying the wood absorbs a substantial amount of power from the microwave field and a minimal amount of energy is transmitted to the water load. However, after that time the converse situation can be observed with a bulk of the energy being transmitted to the load. The computed power absorbed, Fig. 7(b), again appears consistent with the experimentally determined curve, displaying a similar shape and amplitude.

A study of the effect of varying the material location within the waveguide

The results obtained when the wood sample is moved 5 cm forward and 5 cm backward in the over-sized section of the waveguide are depicted by Figs. 8 and 9, respectively. When the material is moved closer to the input source, see Fig. 8, the rate of drying is increased slightly in comparison to the case where the wood is located centrally within the guide, see Fig. 6. Furthermore, there appears to be a more rapid heating along the leading edge of the board, with the temperatures at the points T1 and T7 exhibiting thermal runaway. Nevertheless, the internal

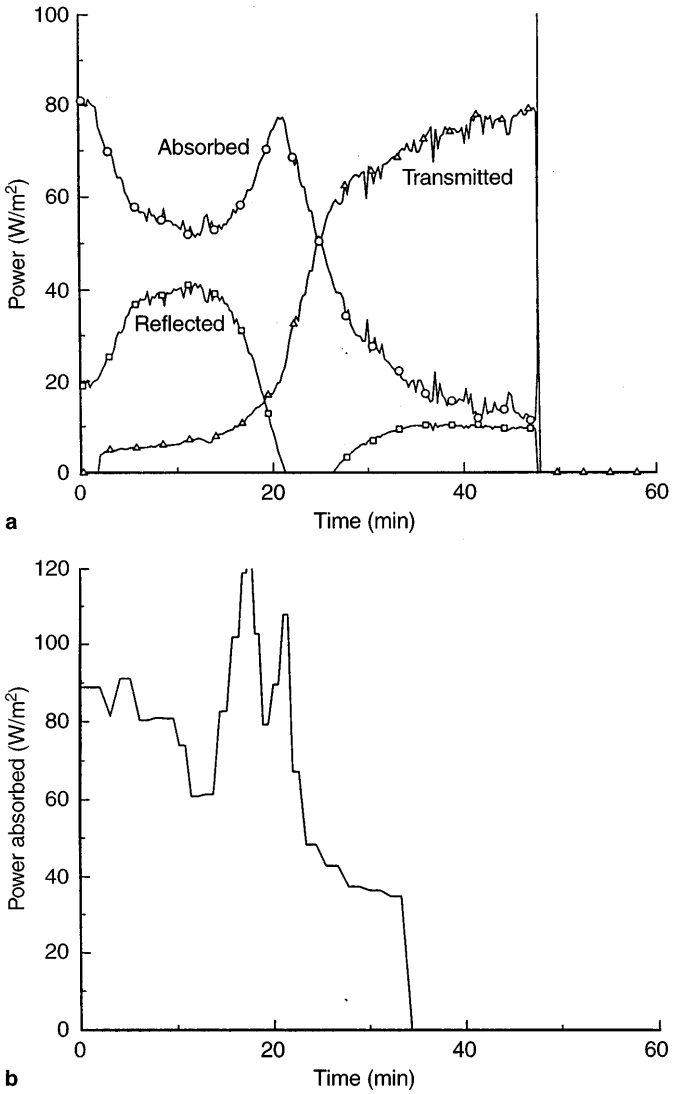

Fig. 7a,b. Comparison between **a** experimentally measured power absorbed and **b** computed power absorbed for combined microwave and convective drying of spruce heartwood

pressure is similar to that observed in Fig. 6. Another observation from Fig. 8 indicates that even the temperature at point T3, near the trailing edge of the board, is higher than was evident when the wood was located in the center of the guide.

In Fig. 9, when the wood sample is moved further away from the input source, it can be seen that the drying kinetics are again different from those generated in Fig. 6. In this case, the temperature at point T1 quickly approaches 200 °C at a rate that is much higher than evident at any other location in the wood. Indeed, for this case, the location within the wood that seems to be the hottest is across the entire central section of the board, rather than along the leading face. Further, the overall internal pressure profiles appear lower than those observed in either Fig. 6 or 8.

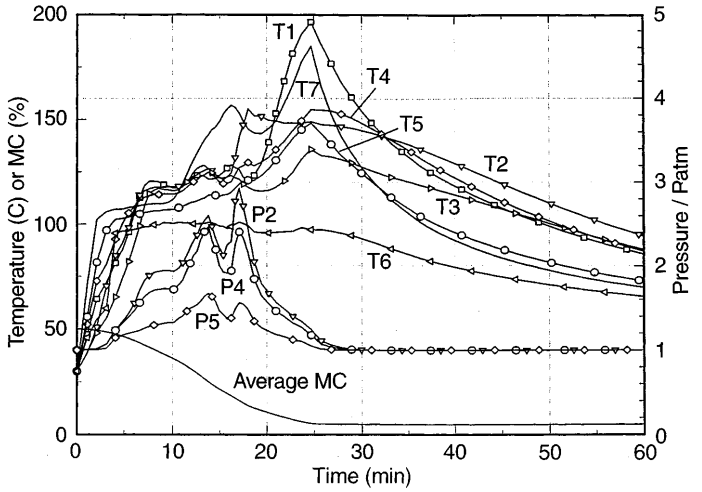

Fig. 8. Simulation results for combined microwave and convective drying of spruce heartwood when the sample is moved 5 cm forward from center in the oversized waveguide

A study of the effect of varying the material size

The drying kinetics that were generated when the size of the wood sample was reduced by 1 cm and then by 2 cm are shown in Figs. 10 and 11, respectively. In Fig. 10, which corresponds to the drying of a sample having dimensions 5.5×6.5 cm (width and half thickness) in the yz-plane, it can be seen that the more intense heating of the wood occurs around the end-piece. In fact, the temperatures across the central plane of the wood, see T1, T2 and T3, show no evidence of thermal runaway, which is inconsistent with what was exhibited in Fig. 6 for the 5.5×7.5 cm sample. Furthermore, and perhaps the biggest difference in comparison with Fig. 6, is the shape and amplitude of the internal pressure profiles.

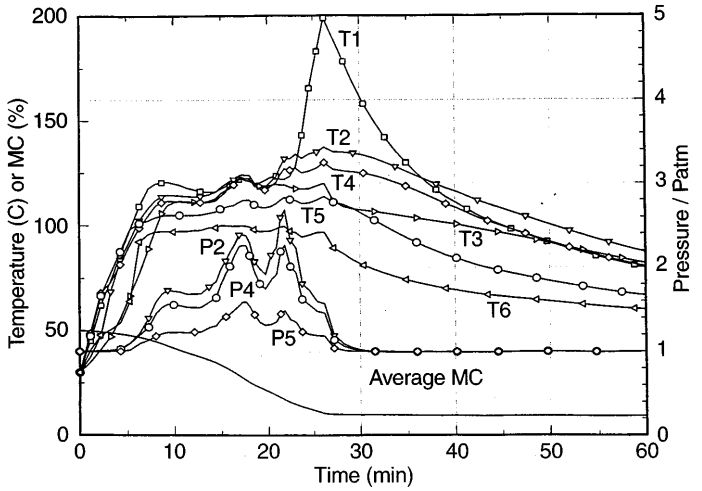

Fig. 9. Simulation results for combined microwave and convective drying of spruce heartwood when the sample is moved 5 cm backward from centre in the oversized waveguide

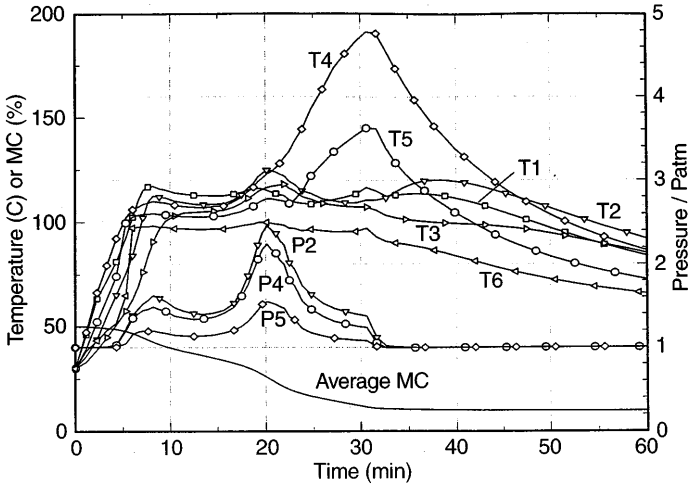

Fig. 10. Simulation results for combined microwave and convective drying of spruce heartwood when the sample length is reduced by 1 cm (5.5 × 6.5 cm in width and half-thickness)

In this case, these profiles show only one distinct peak in pressure, which arises around 20 minutes of drying. This peak is also lower than in Fig. 6.

When the sample is reduced in size a further 1 cm, see Fig. 11, the kinetics in comparison with those depicted in Figs. 6 and 10, change again. Now the peak in the pressure occurs earlier in the drying process and has a behaviour that appears to be the reverse of what was shown in Fig. 10, with the plateau in the pressure occurring after the peak rather than before. Further, the temperatures are lower in this case compared with those shown in Fig. 10, with all of the points around the end-piece (T4 and T5) and even at the surface (T6), exhibiting maxima. The overall drying rate appears to be slightly faster than that exhibited in Fig. 6.

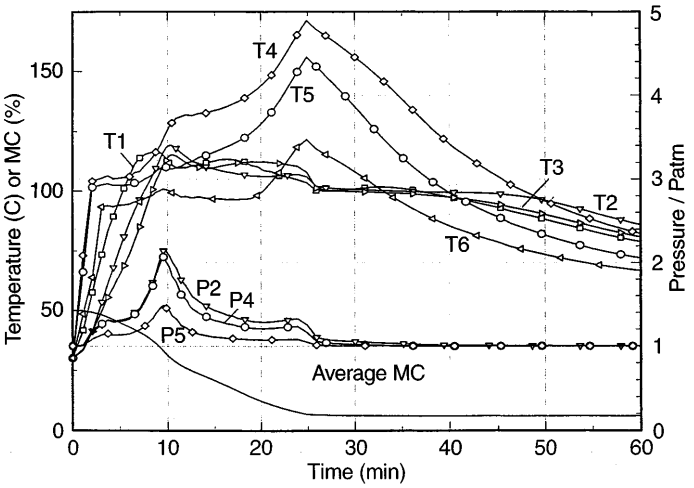

Fig. 11. Simulation results for combined microwave and convective drying of spruce heartwood when the sample length is reduced by 2 cm (5.5 × 5.5 cm in width and half-thickness)

Figure 12 exhibits the carpet plots of the power, temperature, moisture content and pressure fields for the spruce heartwood sample when the y-direction size is

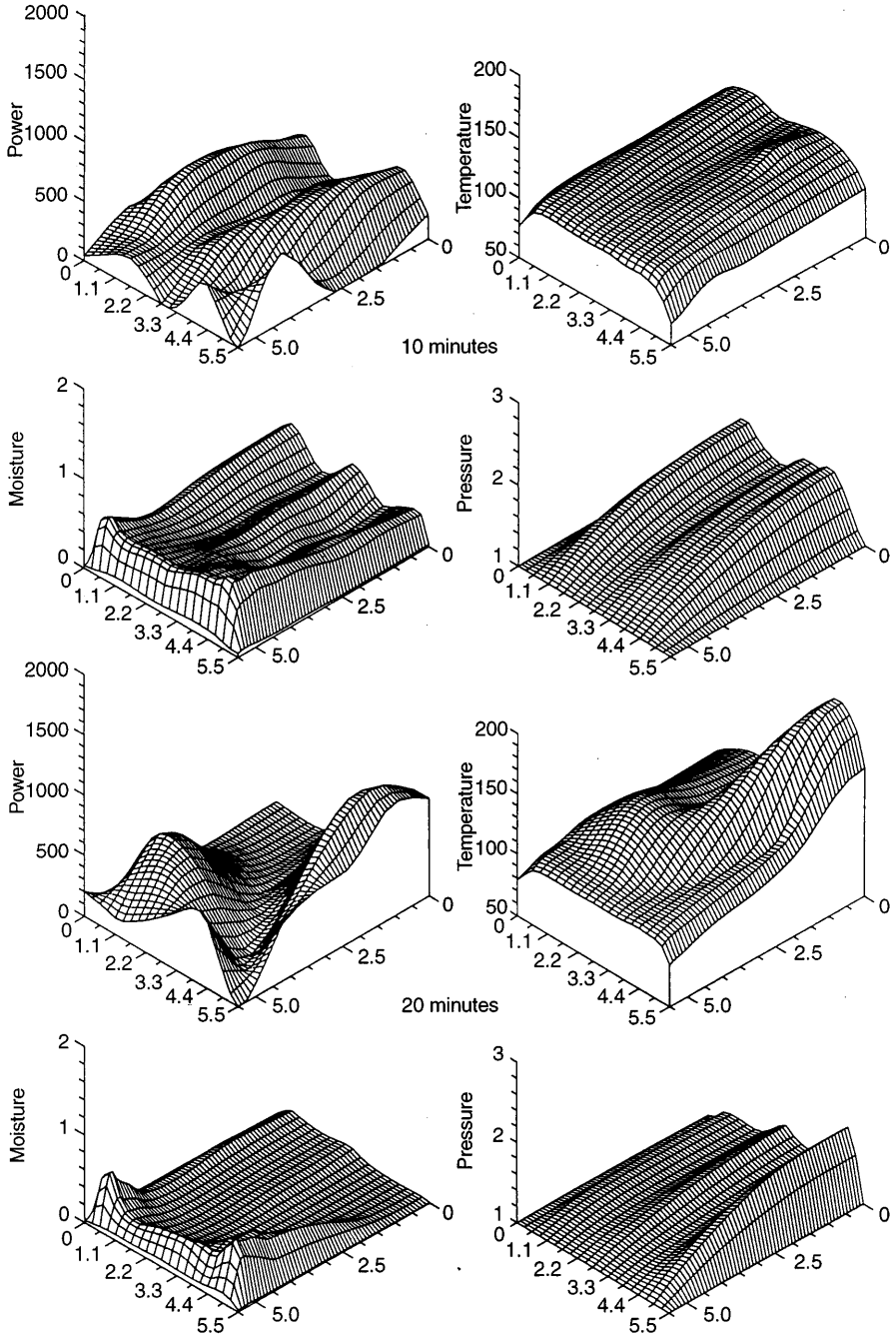

Fig. 12. Carpet plots of the power density, temperature, pressure and moisture content distributions at the times 10 and 20 minutes for the case when the heartwood sample length is reduced by 2 cm

reduced by 2 cm (5.5 × 5.5 cm in width and half-thickness). This figure highlights that the smaller sample has substantially different drying characteristics in comparison with the longer sample shown in Fig. 4. In particular, the power distribution for the smaller sample, after 20 min of drying, appears to be maximising at the centre of the rear section of the board rather than at the leading edge. This maximal power increases the temperature and the pressure around this location. As a direct consequence, the hotspot occurs at the centre of the trailing edge of the board instead of the endpiece, as shown in Fig. 4. The maximum in the total pressure for the smaller sample is lower than depicted in Fig. 4 and also occurs at the rear of the board instead of the middle of the leading edge. These carpet plots again emphasise the effect of sample size when microwave heating is used to assist with the drying process.

The impact of using a short-circuit plane rather than a qave-trap at the end of the guide

In this section, a comparison is made between the kinetics obtained using a water load, see Fig. 6, and a reflective short-circuit plane, see Fig. 13, situated at the end of the wave-guide. Because the water load prevents any reflected energy from back-propagating towards the wood, only forward travelling waves irradiate and subsequently heat the material. However, as a direct result of the energy that is reflected from the leading face of the sample during drying, it is possible that a complicated wave pattern could be generated within the front section of the applicator. Nevertheless, when a short-circuit plane is used within the applicator, backward travelling waves having a different phase and amplitude to the forward travelling waves can arise throughout the entire guide. In this case, the reflected

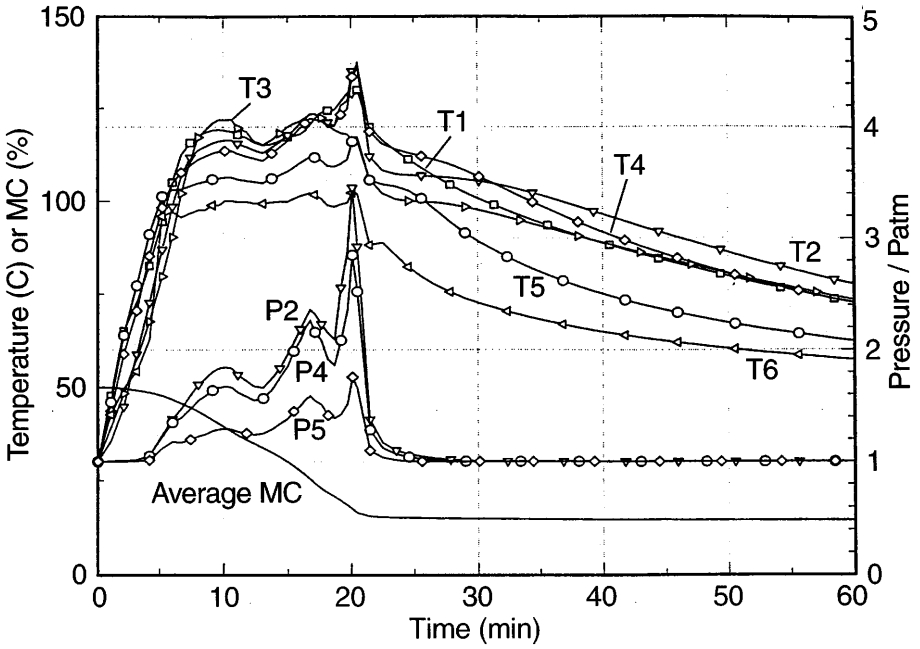

Fig. 13. Simulation results for combined microwave and convective drying of spruce heartwood when a short circuit plane is used instead of a wave trap

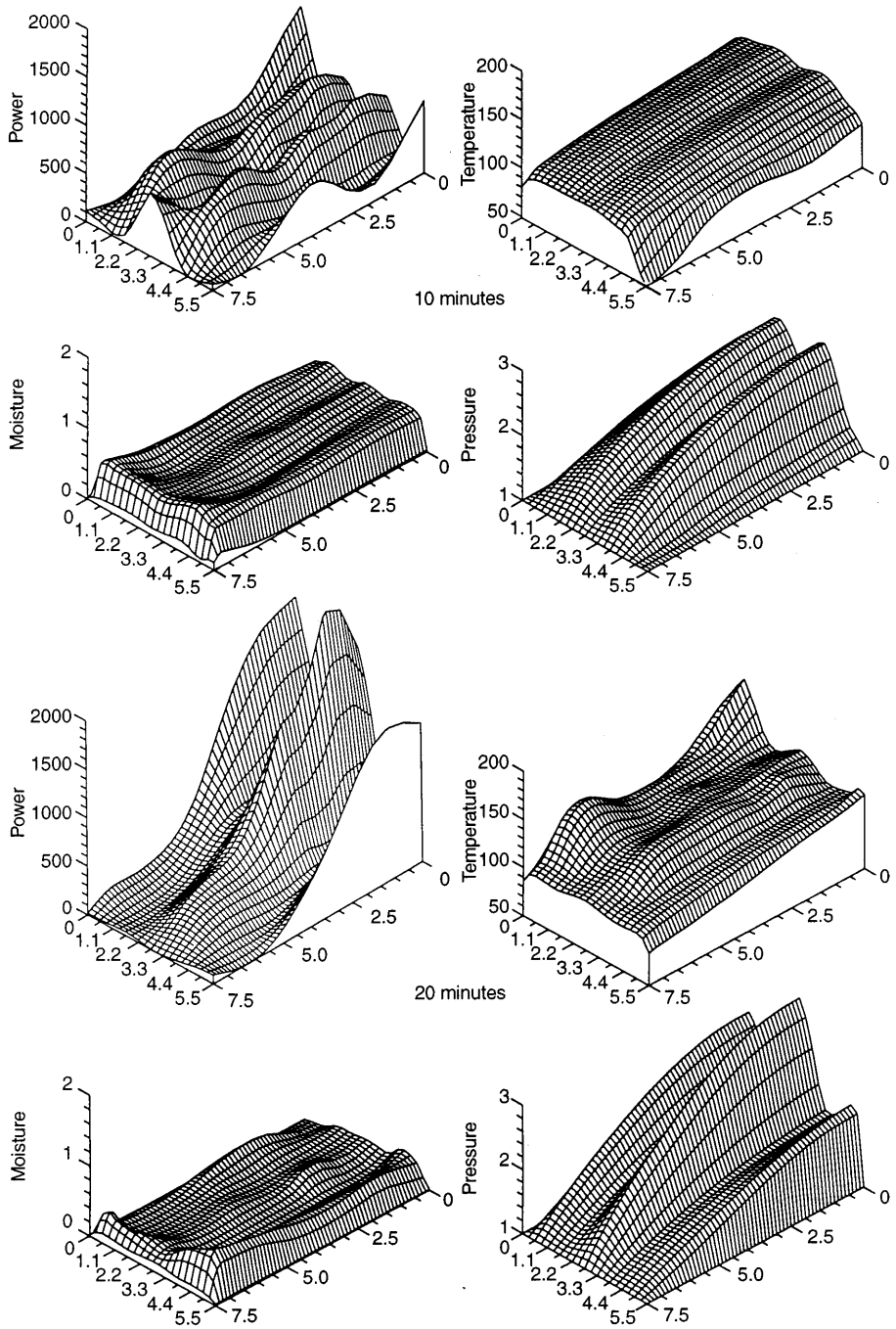

Fig. 14. Carpet plots of the power density, temperature, pressure and moisture content distributions at the times 10 and 20 min for the case when the short circuit plane is used

energy could assistant with heating the trailing face of the wood sample, thus enabling a more uniform heating phenomenon to occur.

From Fig. 13, it seems that the temperature distribution inside the wood for the short-circuit case is indeed more uniform in comparison to the distributions generated for the water-load case in Fig. 6. In fact, closer observation of Fig. 13 highlights that the internal pressures are slightly higher, and the drying time shorter than those shown in Fig. 6. Further, the numerical points that were chosen to display the temperature field show no real evidence of thermal runaway.

Figure 14 depicts the carpet plots associated with this test case study after 10 and 20 minutes of microwave drying. The figure again highlights the differences in the overall drying characteristics when the short circuit plane is used instead of the water load. The main differences between the results shown here and those exhibited in Fig. 4, are the magnitude and shape of the power distribution, the higher and more uniform internal temperatures and the evidence of three distinct pressures peaks within the sample (see carpet plots at 20 min).

Conclusions

It has been shown that the mathematical model that combines a two-dimensional transfer code with a three-dimensional electromagnetic computational scheme, captures the overall behaviour of combined microwave and convective drying of heartwood spruce remarkably well and is able to predict the occurrence of thermal runaway within the material. This result in itself is an important achievement in advancing the knowledge of how microwaves interact with complicated hygroscopic and anisotropic materials, such as wood, throughout microwave heating processes. The model was used thereafter to study in detail some important aspects of microwave enhanced drying.
In particular, the effects of varying the sample location and size within the waveguide have been shown to impact upon the overall characteristics of drying kinetics. This fact highlights that optimising the performance of an over-sized waveguide depends on numerous issues, which indeed, could be investigated using the numerical model proposed here as a real engineering tool. Furthermore, the use of reflective short-circuit plane rather than a water load at the end of the applicator appears to be worthwhile endeavour, because a more uniform temperature distribution, together with a slightly faster drying process results. In summary, it is hoped that the work presented enables the reader to see the powder that mathematical modelling strategies can offer and to conclude that their use, together with experimental verification, is a cost efficient way of advancing microwave technology and optimising existing applicator design specifications.

References

Chen PS, Pei DCT (1987) Microwave heating in drying of hygroscopic materials, IEEE MONTECH′ 87, pp. 72–76
Constant T (1992) Le Séchage Combiné Convection-Micro-Ondes: Modélisation, Validation, Optimisation, Ph.D. Thesis, INPL, Nancy, France
Constant T, Perré P, Moyne C (1996) Drying with Internal Heat Generation: Theoretical Aspects and Application to Microwave Heating. AIChE J. 42(2): 359–368
De Pourcq M (1985) Field and power-density calculations in closed microwave systems by three-dimensional finite differences, IEEE, **132**, part H, (6): 360–368
Dibben DC, Metaxas AC (1994) Finite Element Time Domain Analysis of Multimode Applicators Using Edge Elements. J. Microwave Power and Electromagnetic Energy 29(4): 242–251
Liu F, Turner IW, Bialkowski ME (1994) A Finite-difference time-domain simulation of the power density distribution in a dielectric loaded microwave cavity. J. Microwave Power and Electromagnetic Energy 29(3): 138–148

Liu F, Turner IW (1996) Numerical modelling techniques for simulating the microwave heating of polymer materials inside a ridge waveguide, Proceedings of the Seventh Biennial Conference on Computational Techniques and Applications: CTAC95, Edited by R.L. May and A.K. Easton, World Scientific Publishing Co., pp. 517–524
Liu F, Turner IW, Siores E, Groombridge P (1996) A Numerical and Experimental Investigation of the modelling of the microwave heating of polymer materials inside a ridge waveguide. J. Microwave Power and Electromagnetic Energy 31(2): 71–82
Perré P, Moser M, Martin M (1993) Advances in transport phenomena during convective drying with superheated steam or moist air. Int. J. Heat and Mass Transfer 36(11): 2725–2746
Perré P, Turner IW (1996) A complete coupled model of the combined microwave and convective drying of softwood in an oversized waveguide, Drying' 96, Proceedings of the 10th International Drying Symposium, Krakow, Poland, Vol A: 183–194

Perré P, Turner IW (1996) The use of macroscopic equations to stimulate heat and mass transfer in porous media: some possibilities illustrated by a wide range of configurations that emphasis the role of internal pressure, Mathematical modeling and Numerical Techniques in Drying Technology, pp. 83–156, (edited by I.W. Turner and A. Mujumdar), Marcel Dekker, Inc.
Perré P, Turner IW (1997) Microwave drying of softwood in an oversized waveguide: theory and experiment. AIChE J. under revision
Turner IW, Perré P (1996) A synopsis of the strategies and efficient resolution techniques used for modelling and numerically simulating the drying process, Mathematical modeling and Numerical Techniques in Drying Technology, pp. 1–82, (edited by I.W. Turner and A. Mujumdar), Marcel Dekker, Inc.
Whitaker S (1977) Simultaneous heat, mass and momentum transfer in porous media: a theory of drying. Advances in Heat Transfer 13: 19–203, Academic Press, New York
Zhao H, Turner IW, Liu F (1996) Numerical Simulation of the Power Density Distribution Generated in a Multimode Cavity by Using the Method of Lines Technique to Solve Directly for the Electric Field. IEEE Transactions on Microwave Theory and Techniques 44(12): 2185–2194
Zhao H, Turner IW (1996) An analysis of the finite-difference time-domain method for modelling the microwave heating of dielectric materials within a three-dimensional cavity system. J. Microwave Power and Electromagnetic Energy, December Issue

Appendix

A.1 – Physical formulation used in the code "TRANSPORE"

Notations
Throughout the following, two averaged values are used:

$$\overline{\Psi} = \frac{1}{v_l}\int_{v} \Psi \, dv \quad \text{for the spatial average} \tag{1}$$

$$\text{and} \quad \overline{\Psi}^{i} = \frac{1}{v_i}\int_{v_i} \Psi \, dv \quad \text{for the intrinsic average over phase i} \tag{2}$$

Wood is assumed to be made up of four phases (s = solid, l = liquid, g = gaseous and b = bound water). A bold letter denotes a vector and a sign = denotes a order 2 tensor. The apparent density of the porous media ρ_0 is defined by: $\rho_0 = \overline{r}_s$

Mass conservation equations

$$\text{liquid phase} \qquad \frac{\partial \overline{\rho}_l}{\partial t} + \nabla \cdot (\rho_l \overline{\mathbf{u}}_l) = -\langle \dot{m} \rangle \tag{4}$$

gaseous phase $$\frac{\partial \overline{\rho}_g}{\partial t} + \nabla \cdot (\overline{\rho}_g^g \overline{\mathbf{u}}_g) = \langle \dot{m} \rangle \; + \; \langle \dot{m}_b \rangle \tag{5}$$

vapour only $$\frac{\partial \overline{\rho}_g}{\partial t} + \nabla \cdot (\overline{\rho}_{g_l}^g \overline{\mathbf{u}}_g) = \langle \dot{m} \rangle \; + \; \langle \dot{m}_b \rangle \tag{6}$$

bound water $$\frac{\partial \overline{\rho}_g}{\partial t} + \nabla \cdot (\overline{\rho}_{g_l}^g \overline{\mathbf{u}}_g) = \langle \dot{m} \rangle \; + \; \langle \dot{m}_b \rangle \tag{7}$$

Transport equations

Generalized Darcy's law $$\overline{\mathbf{u}}_g = -\frac{\overline{\overline{\mathbf{K}}}_g \overline{\overline{k}}_{rg}}{\mu_g} \nabla \overline{P}_g^g \tag{8}$$

$$\overline{\mathbf{u}}_l = -\frac{\overline{\overline{\mathbf{K}}}_l \overline{\overline{k}}_{rl}}{\mu_l} \nabla \overline{P}_l^l \tag{9}$$

with $$\overline{P}_l^l = \overline{P}_g^g - P_c \tag{10}$$

bound water diffusion $$\overline{\rho_b \mathbf{u}_b} = -\overline{\overline{D}}_b \nabla \{\overline{\rho}_b\} \tag{11}$$

gaseous diffusion $$\overline{\rho}_v^g \overline{\mathbf{u}}_v = \overline{\rho}_v^g \overline{\mathbf{u}}_g - \overline{\rho}_v^g \overline{\overline{D}}_{eff} \nabla \left\{ \frac{\overline{\rho}_v}{\overline{\rho}_g} \right\} \tag{12}$$

Energy conservation

The enthalpy balance

$$\frac{\partial}{\partial t} \{\overline{\rho h}\} + \nabla \cdot (\overline{\rho \mathbf{u} h}) = \nabla \cdot (\overline{\overline{\lambda}}_{eff} \nabla \overline{T}) \tag{13}$$

gives the equation governing the temperature:

$$\begin{aligned} &\overline{\rho C_p} \frac{\partial T}{\partial t} + \Delta h_{vap} \{\langle \dot{m} \rangle + \langle \dot{m}_b \rangle\} \; + \; h_s \langle \dot{m}_b \rangle - \overline{\rho_b \mathbf{u}_b} \nabla (h_s) \\ &\quad + \left[(\rho_l \overline{\mathbf{u}}_l + \overline{\rho_b \mathbf{u}_b}) C_{pl} + \sum_{i=a,v} (\overline{\rho}_i^g \overline{\mathbf{u}}_i C_{pi}) \right] \cdot \nabla \overline{T} = \nabla \cdot (\overline{\overline{\lambda}}_{eff} \nabla \overline{T}) \end{aligned} \tag{14}$$

Boundary conditions

On a convective surface, the total pressure of the gaseous phase equals the external pressure and heat and mass transfer come from exchange coefficients:

$$\begin{aligned} &\overline{P}_g^g = P_{ext} \\ &[\overline{\overline{\lambda}}_{eff} \nabla \overline{T} + \overline{\rho_b \mathbf{u}_b} h_s + (\rho_l \overline{\mathbf{u}}_l + \overline{\rho_b \mathbf{u}_b}) \Delta h_{vap}] \cdot \mathbf{n} = h(\overline{T}_{surf} - T_\infty) \\ &[\rho_l \overline{\mathbf{u}}_l + \overline{\rho_b \mathbf{u}_b} + \overline{\rho}_v^g \overline{\mathbf{u}}_v] \cdot \mathbf{n} = \ln \left\{ \frac{1 - x_{v\infty}}{1 - x_{vsurf}} \right\} \end{aligned} \tag{16}$$

The expression of external mass flux, which comes from the film theory, tends to infinity in case of pure vapour. This means that the resistance to external moisture transfer equals zero. In this case, $\overline{P_v^g} = P_{ext}$.

A.2 – Physical properties for spruce heart wood

Drying Conditions and Material properties	Values used for the Computations
Initial Moisture Content	50%
Initial Temperature	30 °C
Porosity	0.733
Density of solid Matrix	400 kg m^{-3}
Heat Capacity	$\overline{\rho C_p} = \rho_0(1113 + 4.85T + 4185X)(J\ kg^{-1}\ °C^{-1})$
Vapour pressure	$P_v = P_{vs} \exp\left[\begin{array}{l}(-3.3527 - 0.01328T + 23.63 \times 10^5 T^2) \\ \times (0.8487 - 67.4 \times 10^{-5} T)^{92X}\end{array}\right]$
Capillary pressure	$P_c = 1.364 \times 10^5\ \sigma(X_l + 1.2 \times 10^{-4})$
Gaseous diffusion (R)	$D_{eff} = 10^{-3} \times k_{rg} \times D_v$
(L)	$D_{eff} = 2 \times 10^{-2} \times k_{rg} \times D_v$
Bound water diffusion	$D_b = \exp\left[-9.9 + 9.8X - \frac{4300}{T_k}\right]$
Radial Direction:	
Intrinsic Liquid Permeability	5×10^{-17} m^2
Intrinsic Gas Permeability	1×10^{-17} m^2
Longitudinal Direction:	
Intrinsic Liquid Permeability	5×10^{-14} m^2
Intrinsic Gas Permeability	1×10^{-14} m^2
Wood cross-section (R × L)	5.5 × 7.5 cm
Air Characteristics	Dry Bulb Temperature of 50 °C Wet Bulb Temperature of 35 °C Air Velocity of 2 m s^{-1} Heat Transfer Coefficient 15 W m^{-2} K^{-1} Mass Transfer Coefficient 0.015 m s^{-1}

Liquid moisture content	Relative permeability of the liquid phase	Relative permeability of the gas phase
$X_{wf} = 0$	0	1
Transverse: $0 \le X_{wf} \le X_{sat}$	$\left(\frac{X_{wf}}{X_{sat}}\right)^3$	$1 + \left(2\frac{X_{wf}}{X_{sat}} - 3\right)\left(\frac{X_{wf}}{X_{sat}}\right)^2$
Longitudinal: $0 \le X_{wf} \le X_{sat}$	$\left(\frac{X_{wf}}{X_{sat}}\right)^8$	$1 + \left(4\frac{X_{wf}}{X_{sat}} - 5\right)\left(\frac{X_{wf}}{X_{sat}}\right)^4$